and as in the previous section I study the convergence with chiral order and the cut-off dependence.

differential cross section obtained with ... model of nuclear current. verte

-3 and

3.2 Helium photodisintegration

Three-body ~~Three~~ breaking Helium suggest 4He

3.2.1 ~~3N photodisintegration~~

It has to be discussed:

1). why these configurations and energies

In this section I will discuss results for $^3\text{He} \rightarrow p + p + n$ process.

In the Fig. 3.26 I demonstrate a differential cross section $\frac{d^5\sigma}{d\Omega_1 d\Omega_2 dS}$ as a function of the S arc length. The photon energy is $E_\gamma = 30\,\text{MeV}$; ~~and~~ the kinematic configuration $\theta_1 = 15°$, $\phi_1 = 0°$, $\theta_2 = 15°$, $\phi_2 = 180°$; predictions have been obtained without 3NF. ~~We~~ On the left we see that only NLO and N^{2}LO introduce relatively large truncation error. The maximal width of a band for NLO is 37.6 % at $S = 10\,\text{MeV}$, for N^{2}LO it is 12.4 % at the same ~~point~~ S value and it is gradually decreasing coming to 0.13 % at N^{4}LO$^+$. The cutoff spread (right) around maxima values ~~is less than~~ but remains below 3 %. ~~and~~ It ~~is~~ reaches 0.78 % at the minimum point ($S = 10\,\text{MeV}$). is biggest

2). why only NN force. Is 3He bound state also calculated without 3NF. ? Do we know, what will change after inclusion of 3NF?

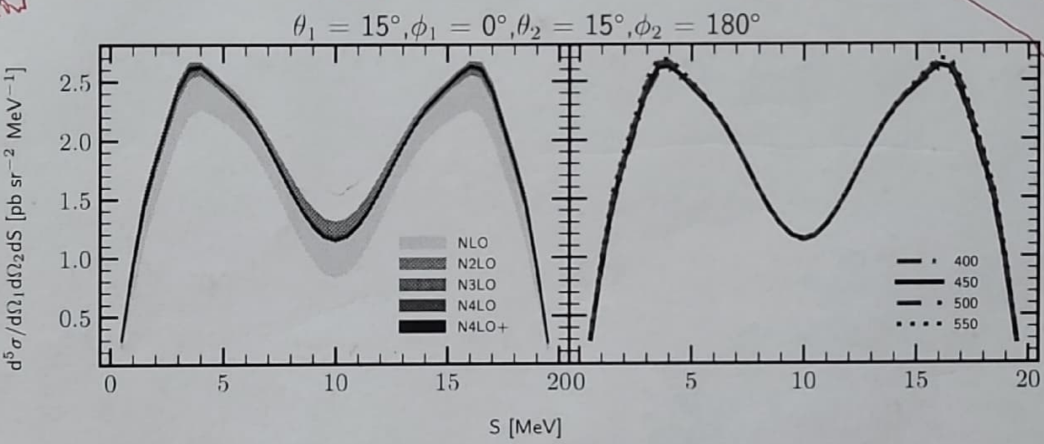

Figure 3.26: The five-fold differential cross section for the photon energy $E_\gamma = 30\,\text{MeV}$ for the kinematic configuration $\theta_1 = 15°$, $\phi_1 = 0°$, $\theta_2 = 15°$, $\phi_2 = 180°$. The left figure presents truncation error bands obtained using the SMS potential with chiral orders from NLO to N^{4}LO$^+$, and with cutoff parameter $\Lambda = 450\,\text{MeV}$. The right figure presents a cutoff dependence at N^{4}LO$^+$. Results are obtained with two-nucleon force only, and ... current model.

for the same $E_\gamma = 100$ MeV

With larger energy $E_\gamma = 100\,\text{MeV}$, for which predictions are demonstrated in the Fig. 3.27, both truncation error and cutoff spread become larger. The truncation band at the maximum point at $S = 10\,\text{MeV}$ for NLO is 55.0 % decreasing to 2.2 % at N^{4}LO$^+$ which still is around 3 times larger than it was ~~in~~ for predictions ~~with~~ at $E_\gamma = 30\,\text{MeV}$. The cutoff spread also becomes larger with increasing energy value: 9.0 % at the same (maximum) point which is also ~ 3 times bigger than the one we observed for the lower energy.

Reults for other angular configurations at $\theta_1 = 75°$, $\phi_1 = 75°$, $\theta_2 = 75°$, $\phi_2 = 105°$ A are ~~demonstrated~~ given in Fig. 3.28. The top row shows results obtained with 2NF only, while predictions obtained with 3NF are shown on the bottom row. It seems that 3NF does not change much the convergence with respect to the chiral order: truncation error band at the point of maximum $S = 35\,\text{MeV}$ (N^{4}LO$^+$) is 1.11 % and 1.16 % with and without 3NF, respectively. ~~So~~ ~~As~~ It is almost the same, ~~meaning that 3NF contribution arising starting from N^{2}LO order~~ does not affect chiral order convergence ~~much~~. Note, 3NF at N^{2}LO has been used for all NN forces above NLO.

The cutoff dependence, in turn, is practically affected by the 3NF presence. Predictions with 2NF only have 13.7 % spread at the same maximum point $S = 35\,\text{MeV}$, while predictions with 3NF have only 1.23 % relative spread, so the difference is tremendous. I conclude that inclusion N^{2}LO 3NF

For giving directions of two momenta $\hat{p}_1$ and $\hat{p}_2$

For three free nucleons in the final state it is convenient to introduce, ~~the arc~~ as a kinematical variable, the arc-length of the S-curve, ~~~~ The S-curve is spanned in the plane defined by kinetic energies of the same two nucleons, E_1 and E_2.

For three particles and known initial ~~~~ energy and momentum ~~the~~ five kinematical variables* are required to define the final kinematics.

* footnote { among nine variables describing final state $\vec{p}_1, \vec{p}_2$ and $\vec{p}_3$ ~~~~ four can be fixed from energy and momentum conservation laws. }

We choose four variables as directions of outgoing nucleons no 1 and 2 : $\theta_1, \varphi_1, \theta_2$ and φ_2, with the $\hat{z}$ axis defined by ~~initial~~ photon momentum.

Choosing E_1 as the fifth variable would introduce ~~~~ ambiguity, as in some cases two ~~~~ values of E_2 could be allowed. Instead, the ~~S-curve~~ location on the S-curve defines the kinematical configuration unambiguously.

The various possible locations of the S-curve in E_1-E_2 plane, as well as the convention on choosing the $S=0$ point is given in Fig.... of Ref. [Glöckle_report].

I'm now not sure if there is an introduction of the S-curve in other chapters. If it is so maybe above description is not needed.

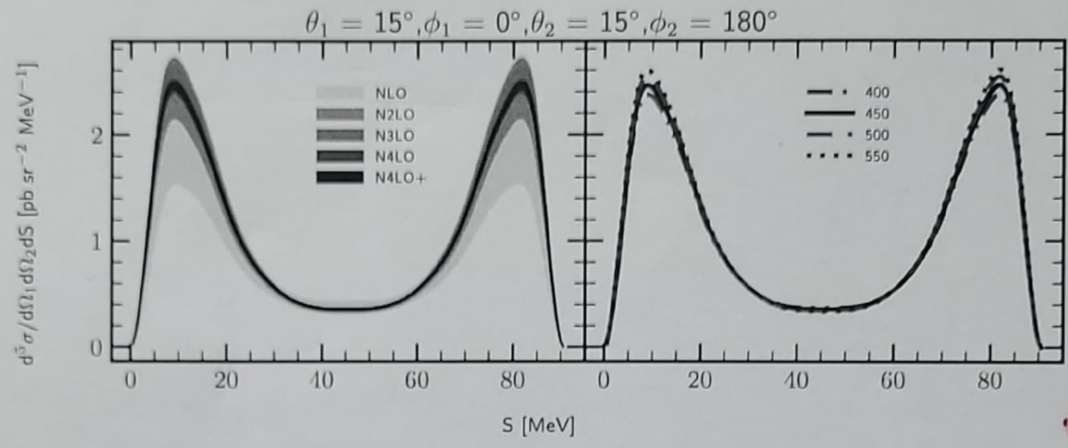

detected

Figure 3.27: The same as in Fig. 3.26 but for the photon energy $E_\gamma = 100$ MeV

Similar trends are present also in other configurations, demonstrated for the comparison: Figs.3.29, Figs.3.30 and Figs.3.31.

~~The~~ semi-inclusive differential cross section $\frac{d^3\sigma}{d\Omega_p dE_p}$ as a function of the outgoing protons energy E_p, ~~is demonstrated on the Fig. 3.32 (for~~ I choose the same photon energies as above: $E_\gamma = 30$ MeV and ~~Fig. 3.33 (for~~ $E_\gamma = 100$ MeV. Each figure consists of subfigures where each row presents results for a proton ~~angles~~ angle $\theta_p = 10°, 50°, 90°, 130°$ and $170°$. The left part of each subfigure shows ~~a~~ the chiral order dependence while the right ~~-~~ the cutoff dependence.

momentum plane

At the photon energy 30 MeV the chiral dependence is relatively weak: at the maximum point ($E_p \simeq 3.8$ MeV) the relative difference varies between 12 % and 28 % at LO for different angles. This difference decreases with each subsequent order resulting in 0.15 % at N^4LO+. At the energy $E_\gamma = 100$ MeV truncation errors are larger: at the maximum around $E_p \simeq 1.46$ MeV the discrepancy is around 40 % (NLO), 15 % (N2LO), coming to 1.5 % at N^4LO^+.

minimum?
maximum?
average?
typical?

~~The~~ cutoff uncertainty at $E_\gamma = 30$ MeV is around 2 % and at $E_\gamma = 100$ MeV ~~is around~~ increases up to 8 % for all angles and at the same values of E_p as regarded above.

Observed small uncertainties allow me to conclude that the semi-inclusive cross section $\frac{d^3\sigma}{d\Omega_p dE_p}$ is not useful in studies aiming on pin-down the ~~this~~ details of the third force. Do we have prediction with other current?

A typical

The exclusive ~~measurements~~ cross sections shown ~~above in~~ above, in Figs 3.26 - 3.31 are small and unfortunately below the possibilities of current ~~experimental~~ experimental techniques. The semi-inclusive measurement is more likely to be performed, thus in Figs 3.32 and 3.33 I show the semi-inclusive ...

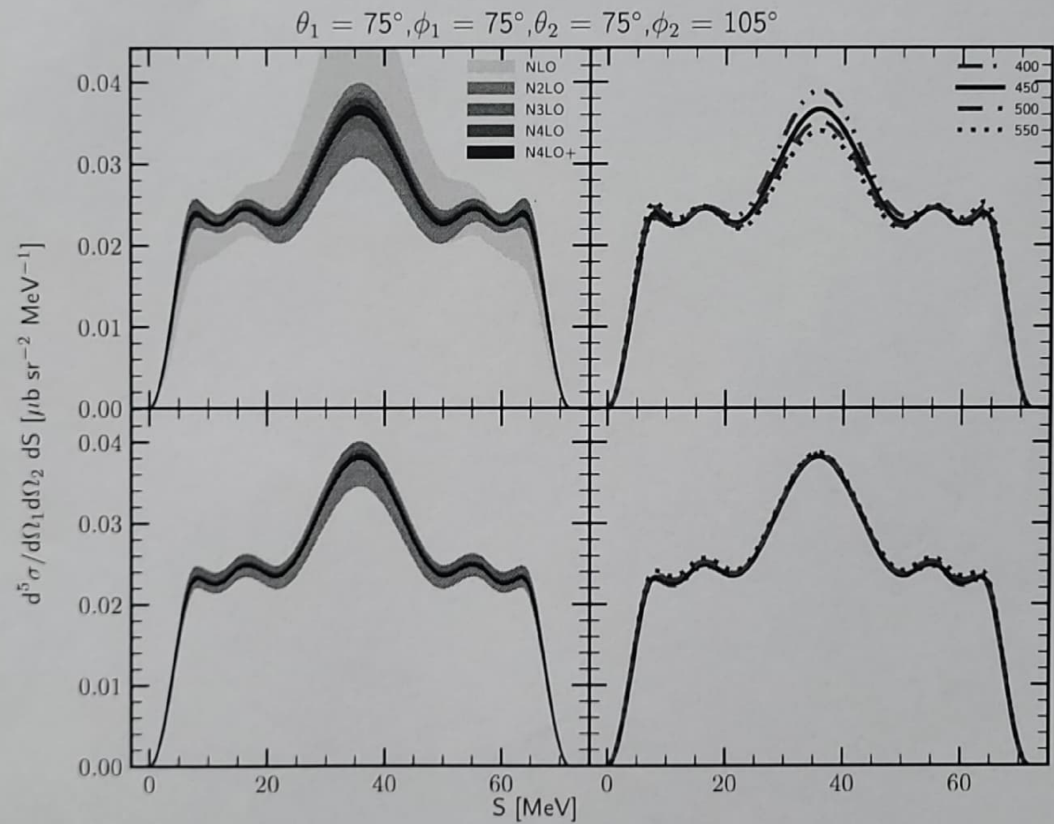

or in?

Figure 3.28: The same as in the Fig. 3.27 but for the ~~different~~ kinematic configuration at $\theta_1 = 75°$, $\phi_1 = 75°$, $\theta_2 = 75°$, $\phi_2 = 105°$. Results obtained with 2NF are presented on the top row. The same, but with 3~~NF~~ is presented on the bottom row (starting from the N^2LO - where 3NF appears.)

and

the chiral SMS 2N force

for the first time.

the N^2LO 3NF included

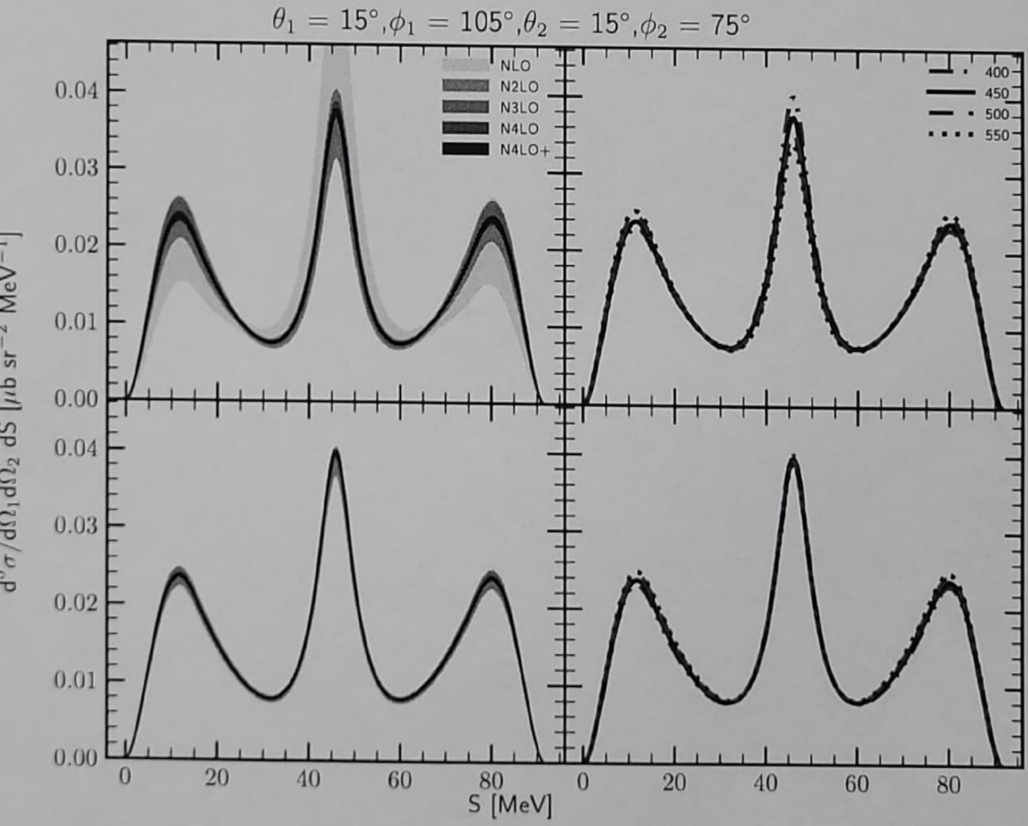

Figure 3.29: The same as in the Fig. 3.28 but for the ~~different~~ kinematic configuration, at $\theta_1 = 15$ - ...... $\theta_2 = 75°$.

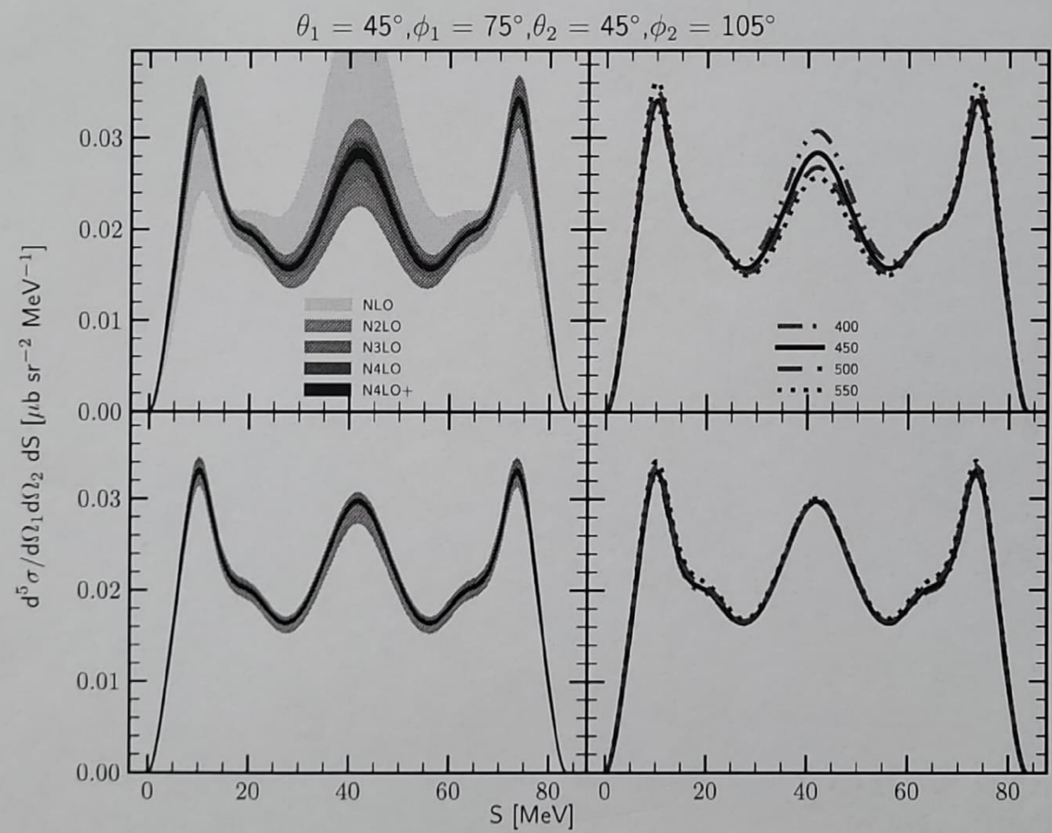

Figure 3.30: The same as in the Fig. 3.29 but for the different kinematic configuration.

Ack changes as in 3.29

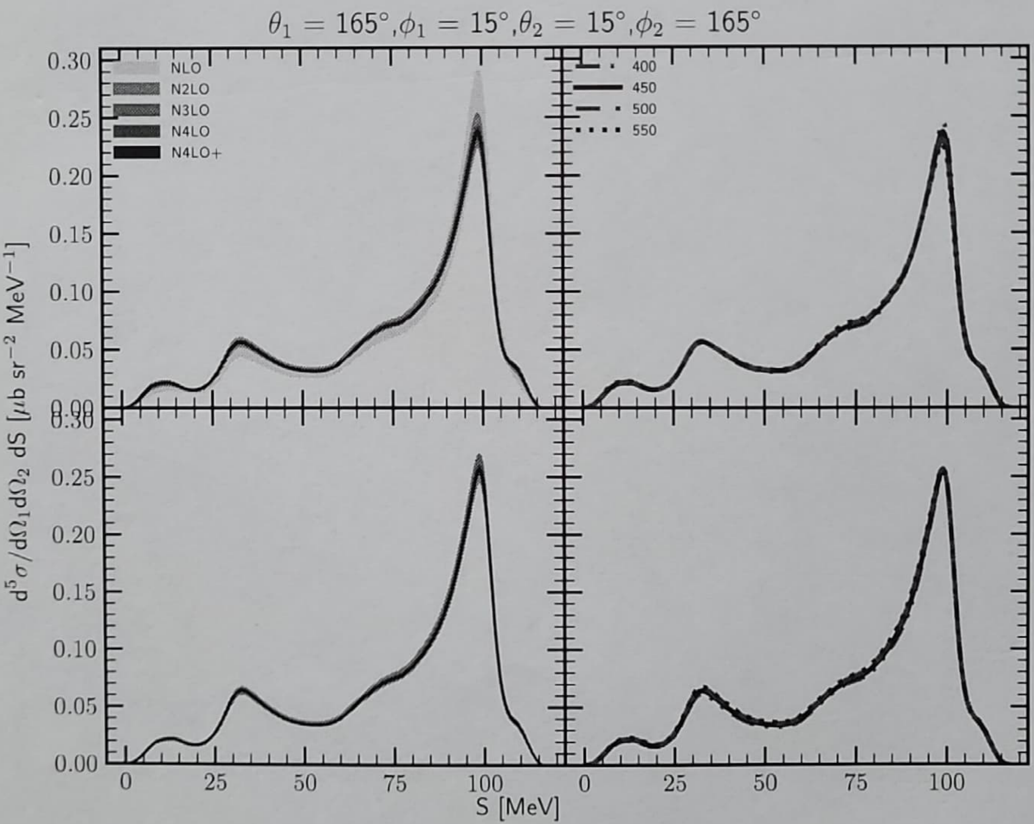

Figure 3.31: The same as in the Fig. 3.30 but for the different kinematic configuration.

Changes as in 3.29

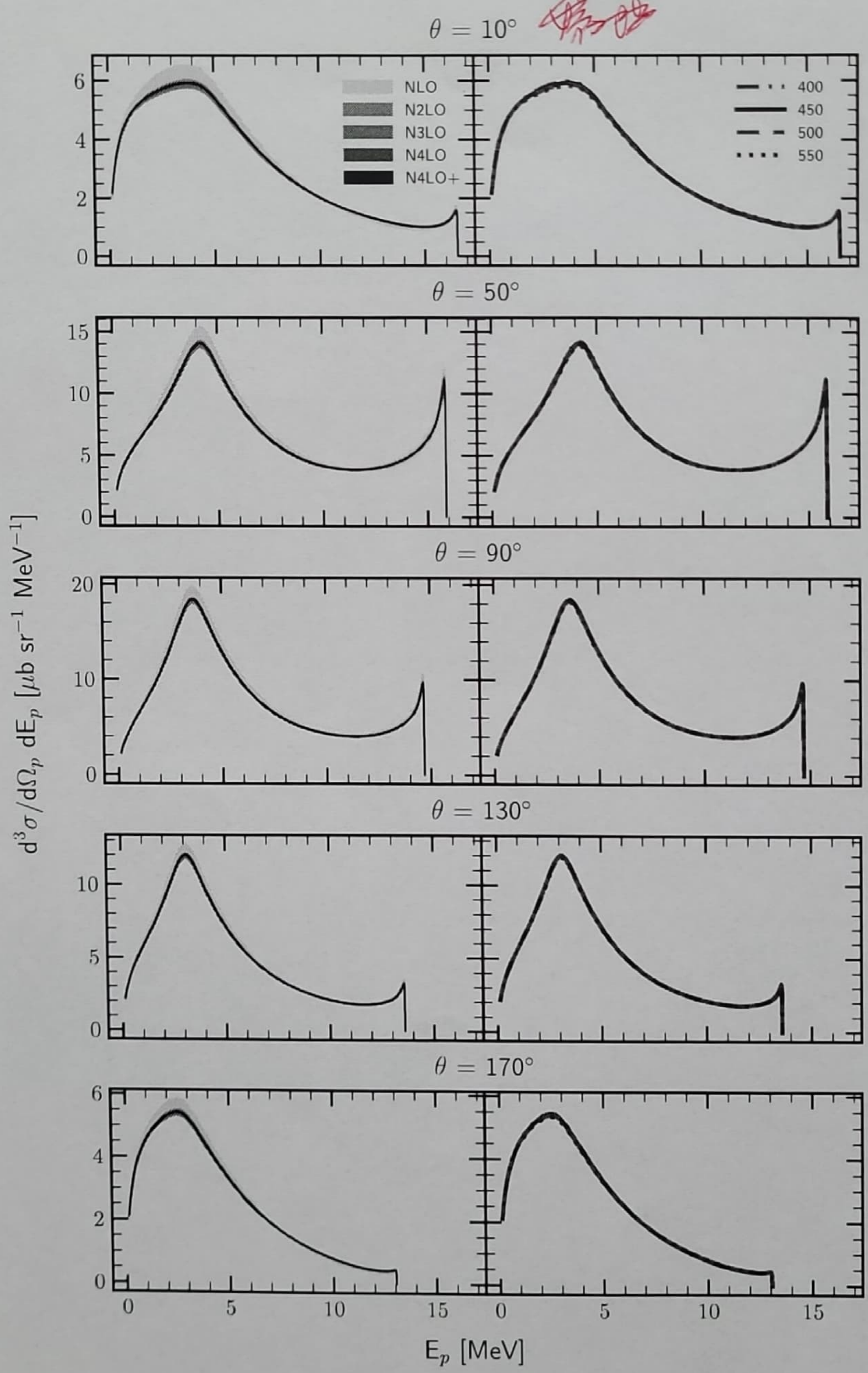

$\varphi_A = 0^\circ$

Figure 3.32: The semi-inclusive differential cross section $\frac{d^3\sigma}{d\Omega_p dE_p}$ at $E_\gamma = 30\,\mathrm{MeV}$ as a function of outgoing proton energy E_p. Each row represents predictions for different values of the outgoing proton's momentum polar angle θ_p: 10°, 50°, 90°, 130° and 170°. ~~Each column has similar curves and bands definitions as it was for exclusive cross section in Fig. 3.26.~~ Predictions have been obtained with the SMS NN potential but neglecting 3NF.

describe

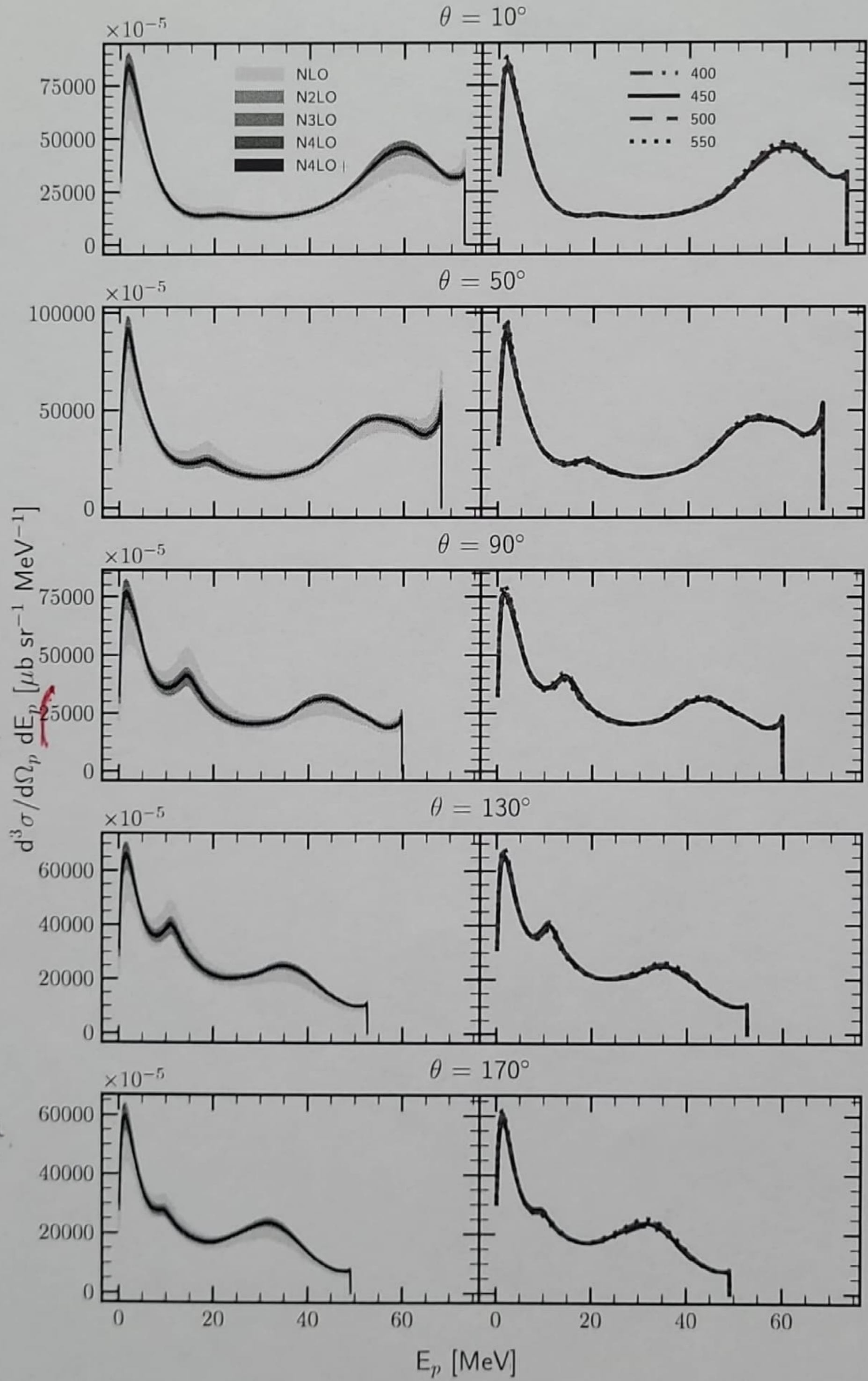

move axis title

~~Are the units correct? Is the cross section much bigger at E_γ=100 MeV than at E_γ=30 MeV? Please check (both figures)~~

Figure 3.33: The same as in Fig. 3.32 but for $E_\gamma = 100\,\mathrm{MeV}$.

Ok there is 10^{-5}! Maybe change to pb$\cdot 10^5$ to avoid long numbers? But check if that magnitudes are in quantitative agreement with paper or my thesis.

a significant inlargment of

3.2.2 ~~D-p photodisintegration~~ Two-body breakup

The differential cross section $d\sigma/d\Omega_d$ for the $^3He + \gamma \rightarrow d + p$ reaction is presented In the Fig. 3.34 (for the photon energy $E_\gamma = 30\,\mathrm{MeV}$) and In the Fig. 3.35 (for ~~the photon energy~~ $E_\gamma = 100\,\mathrm{MeV}$). We see ~~that~~ both truncation and cutoff uncertainties ~~are larger~~ with increasing photon energy. The relative spread of the truncation error at the maximum point ($\theta_p = 105°$) for the lower energy is 0.05 % at N^{4}LO$^+$, while for the larger energy similar spread is 0.45 % (at N^{4}LO$^+$, $\theta_p = 120°$).

The cutoff dependence is also stronger for the larger energy: it is 1.45 % at 30 MeV and 4.01 % at 100 MeV (at the points of maximum).

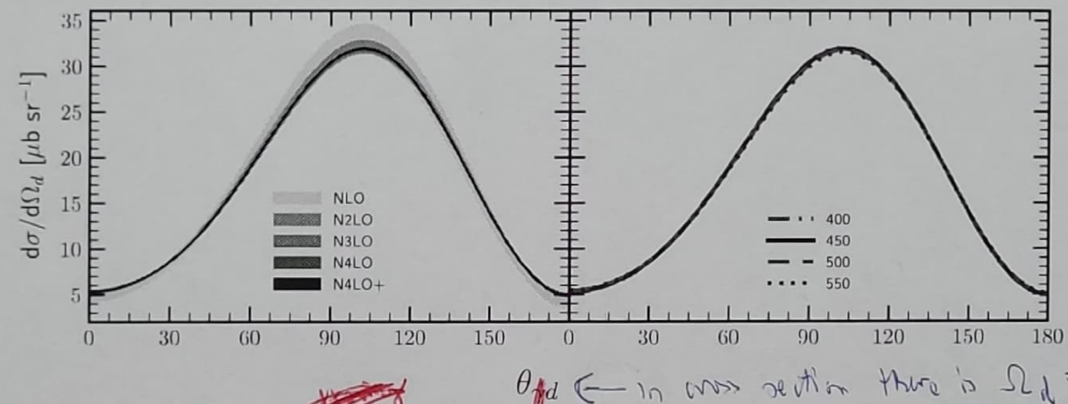

← in cross section there is $\Omega_d = (\theta_d, \varphi_d)$

d-γ in c.m.?

Figure 3.34: Differential cross section for the ~~D-p~~ two-body photodisintegration of ^{3}He as a function of the dγ angle. The initial photon energy $E_\gamma = 30\,\mathrm{MeV}$. NN or NN+3NF ? current ?

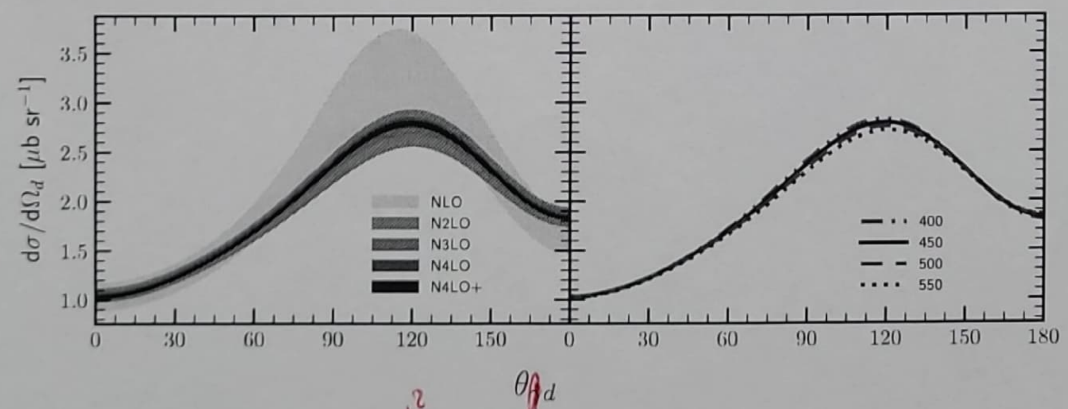

←

in the

Figure 3.35: The same as ~~on~~ Fig. 3.34 but for the photon energy $E_\gamma = 100\,\mathrm{MeV}$,

in the case two neutrons are detected and similarly to the previous chapter I present the convergence of predictions and their cut-off dependence.

3.3 Triton photodisintegration

present

In this section I will discuss results for ${}^3\mathrm{H} + \gamma \rightarrow p + n + n$ process.

In the Fig. 3.36 I ~~demonstrate~~ a differential cross section $\frac{d^5\sigma}{d\Omega_1 d\Omega_2 dS}$ as a function of the S arc length. The photon energy is $\mathrm{E}_\gamma = 30\,\mathrm{MeV}$ and the kinematic configuration $\theta_1 = 15°$, $\phi_1 = 0°$, $\theta_2 = 15°$, $\phi_2 = 180°$; predictions have been obtained without 3NF. We see that only NLO and N^{2}LO introduce relatively large truncation error. The maximal width of a band for NLO is 30.95 % at $S = 10\,\mathrm{MeV}$, for N^{2}LO it is 6.79 % at the same point and it is gradually decreasing coming to 0.10 % at N^{4}LO$^+$. The cutoff spread around maxima values is 6.25 % (at $S = 4\,\mathrm{MeV}$) and it is 1.81 % at $S = 10\,\mathrm{MeV}$.

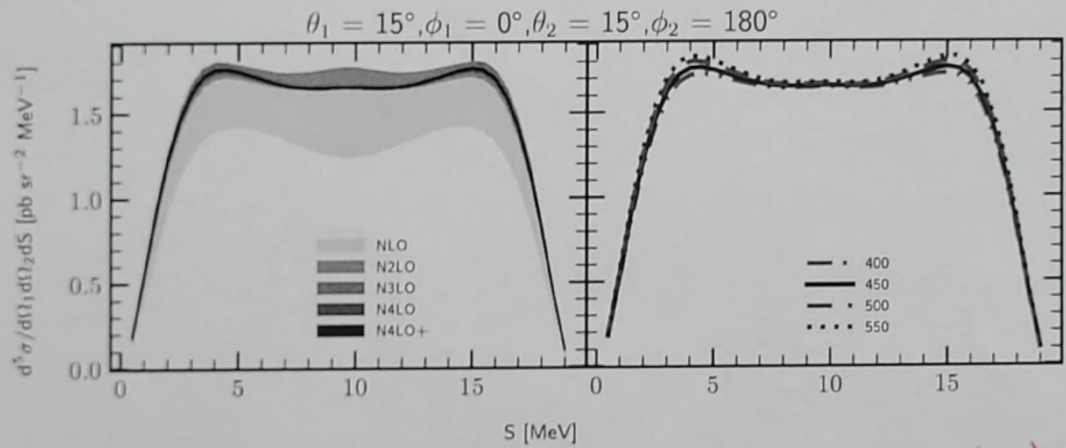

please check in code if that is true

the

with two neutrons detected

Figure 3.36: The five-fold differential cross section for the photon energy $\mathrm{E}_\gamma = 30\,\mathrm{MeV}$ for the kinematic configuration $\theta_1 = 15°$, $\phi_1 = 0°$, $\theta_2 = 15°$, $\phi_2 = 180°$. The left figure presents truncation error bands obtained using potential with chiral orders from NLO to N^{4}LO$^+$, and with cutoff parameter $\Lambda = 450\,\mathrm{MeV}$. The right figure presents a cutoff dependency at N^{4}LO$^+$. Results are obtained with the SMS two-nucleon force only. current?

At bigger

~~With larger~~ energy ~~demonstrated~~ on $\mathrm{E}_\gamma = 100\,\mathrm{MeV}$ demonstrated in the Fig. 3.37, the truncation band at the maximum point $S = 10\,\mathrm{MeV}$ for NLO is 50.26 % decreasing to 2.00 % at N^{4}LO$^+$. The cutoff spread also becomes larger with increasing energy value: 9.52 % at the same maximum.

The truncation error bands and cutoff dependance is very similar ~~as it was~~ to what was found for the three-body ^{3}Helium photodisintegration 3.21 and the relative errors have a similar ~~range of values~~ magnitudes.

Results for other angular configurations and at $\theta_1 = 75°$, $\phi_1 = 75°$, $\theta_2 = 75°$, $\phi_2 = 105°$ are demonstrated in Fig. 3.38 with $\mathrm{E}_\gamma = 30\,\mathrm{MeV}$. Both truncation errors and cutoff dependance are ~~lower~~ smaller at this configuration: the relative width of the truncation band at NLO is 9.39 % (at the maximum point $S = 8\,\mathrm{MeV}$) and drops to only 0.1 % at N^{4}LO$^+$. The relative cutoff spread is 0.93 % at the same point.

bigger

At the ~~larger~~ energy $\mathrm{E}_\gamma = 100\,\mathrm{MeV}$ demonstrated in Fig. 3.39 uncertainties ~~have been increased~~ grows. The truncation bands are 44.42 % and 2.09 % (at NLO and N^{4}LO$^+$, respectively) and the cutoff spread is 13.04 % (all at $S = 35\,\mathrm{MeV}$).

Similar trends are present also in other configurations, demonstrated for the comparison: Figs. 3.40, 3.41, 3.42, 3.43, 3.44 and 3.45.

in maximum

in Figs 3.40 – 3.45

examples

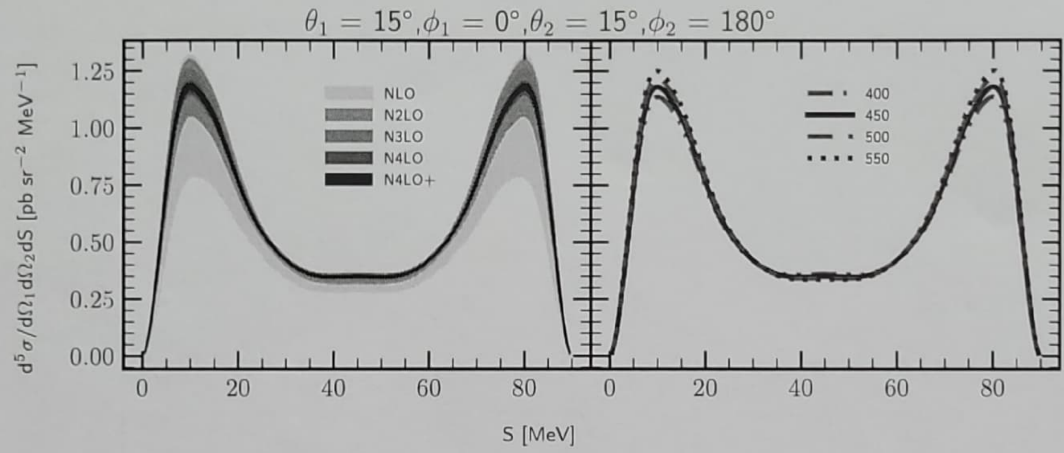

Figure 3.37: The same as in the Fig. 3.36 but for the photon energy $E_\gamma = 100\,\mathrm{MeV}$.

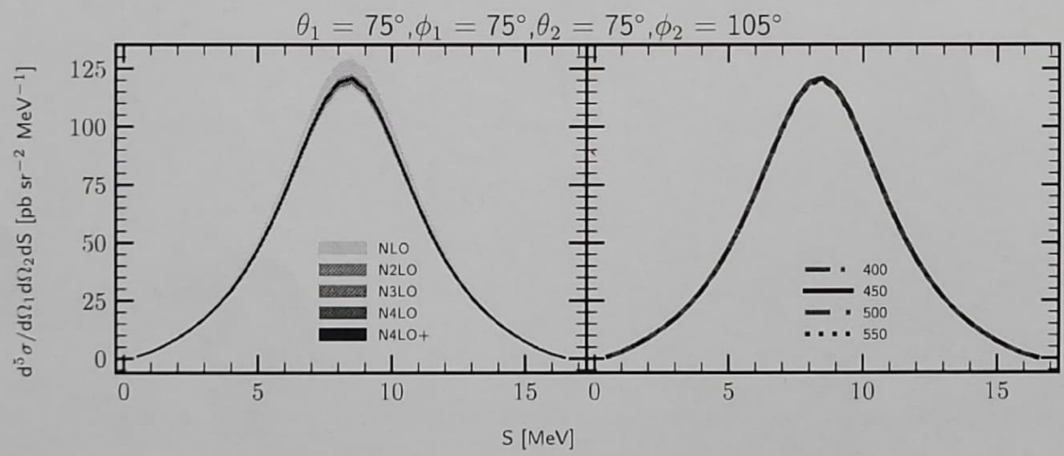

Figure 3.38: The same as in the Fig. 3.36 but for the ~~different~~ kinematic configuration with $\theta_1 = 75°$, $\phi_1 = 75°$, $\theta_2 = 75°$, $\phi_2 = 105°$. ~~Results obtained with 2NF only~~.

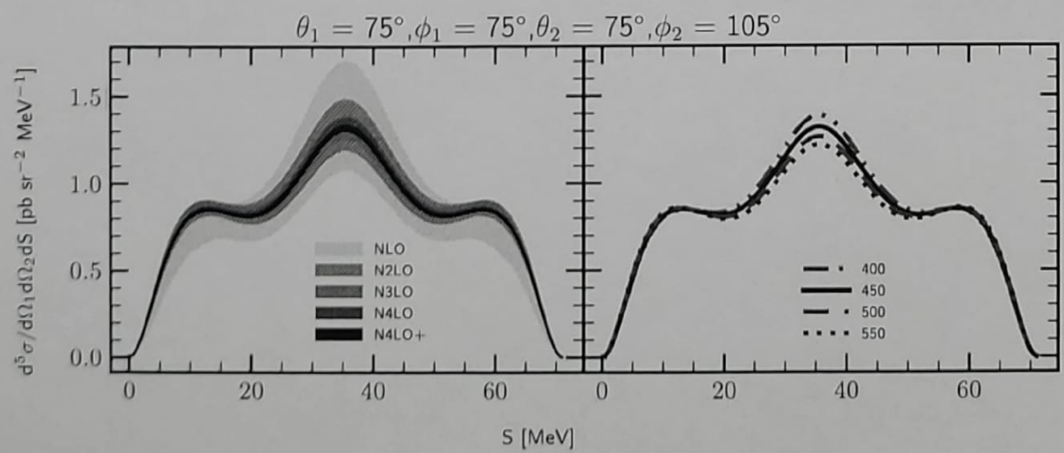

Figure 3.39: The same as in the Fig. 3.38 but for the photon energy $E_\gamma = 100\,\mathrm{MeV}$.

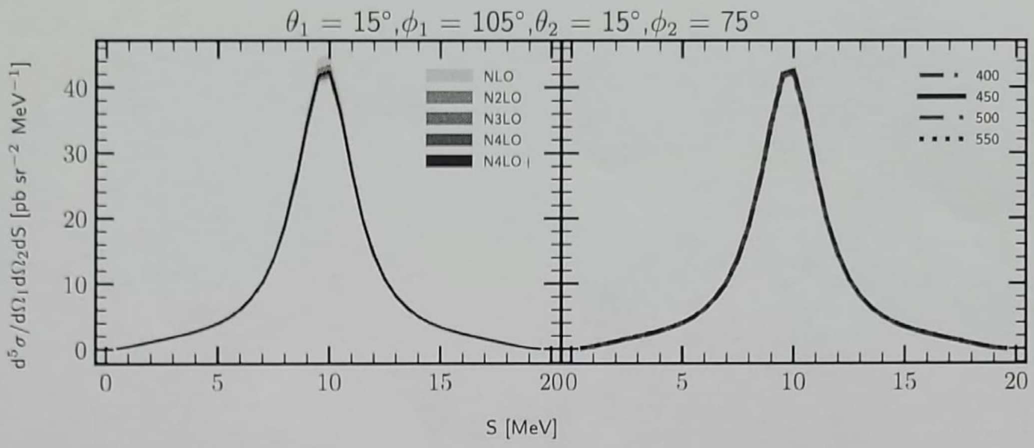

Figure 3.40: The same as in the Fig. 3.38 but for the ~~different~~ kinematic configuration $\theta_1 = 15°$, $\phi_1 = 105°$, $\theta_2 = 15°$, $\phi_2 = 75°$. Results ~~obtained with 2NF only.~~ wM

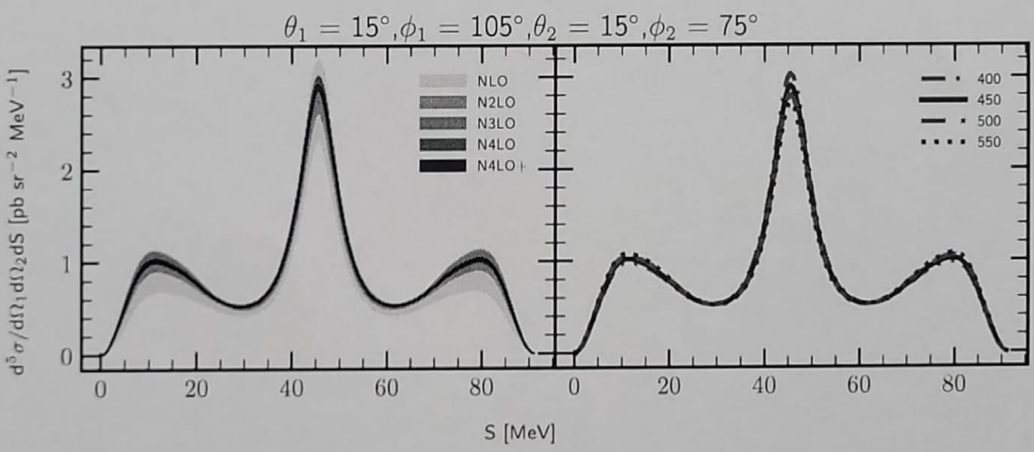

Figure 3.41: The same as in the Fig. 3.40 but for the photon energy $E_\gamma = 100\,\mathrm{MeV}$.

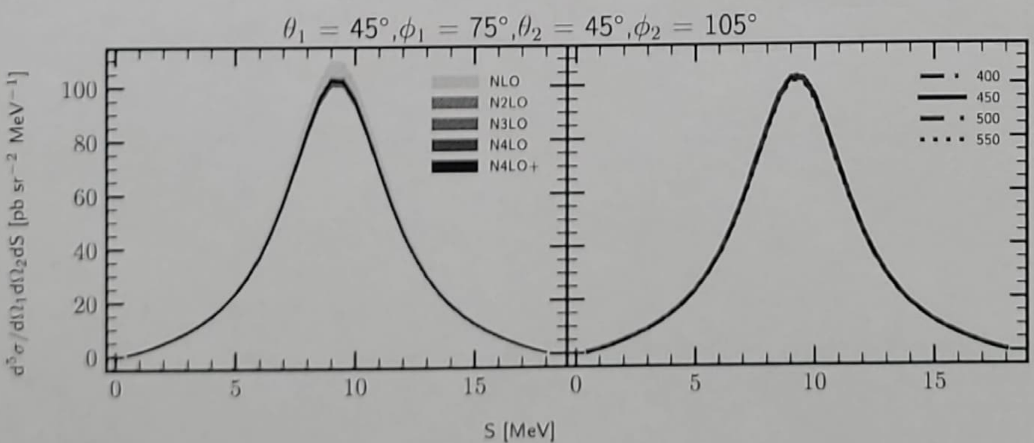

Figure 3.42: The same as in the Fig. 3.40 but for the ~~different~~ kinematic configuration $\theta_1 = 45°$, $\phi_1 = 75°$, $\theta_2 = 45°$, $\phi_2 = 105°$. Results ~~obtained with 2NF only.~~ wM

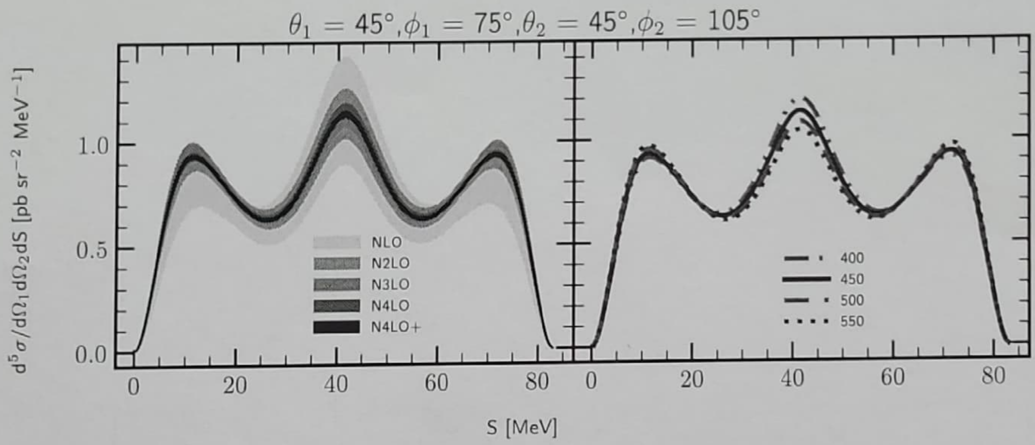

Figure 3.43: The same as in the Fig. 3.42 but for the photon energy $E_\gamma = 100\,\text{MeV}$.

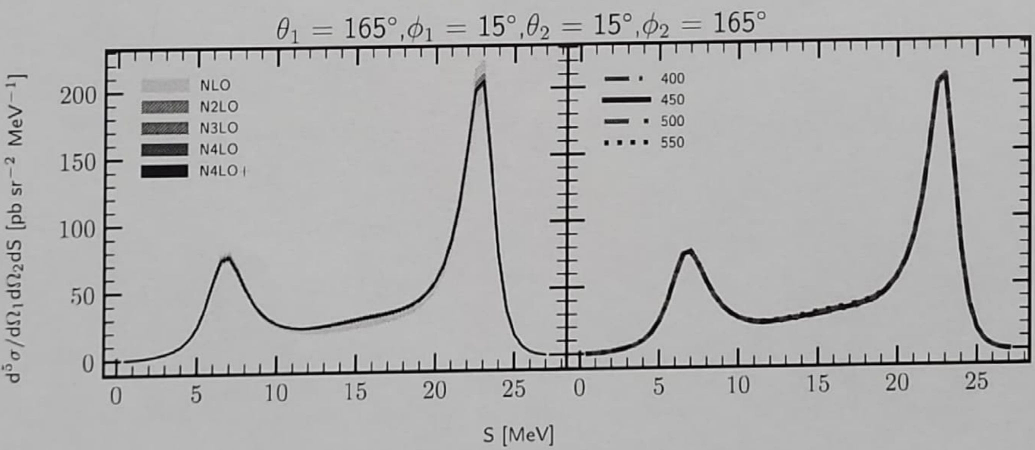

Figure 3.44: The same as in the Fig. 3.42 but for the ~~different~~ kinematic configuration with $\theta_1 = 165°$, $\phi_1 = 15°$, $\theta_2 = 15°$, $\phi_2 = 165°$. ~~Results obtained with 2NF only.~~

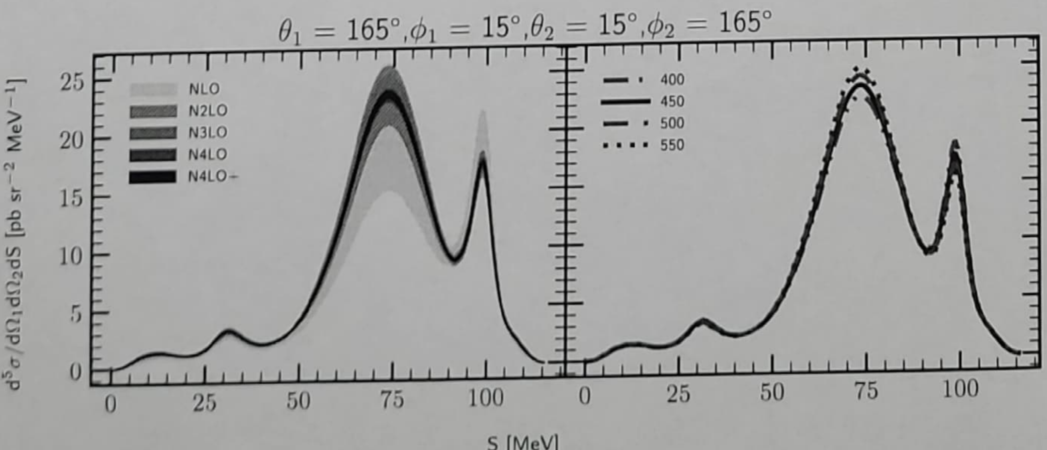

Figure 3.45: The same as in the Fig. 3.44 but for the photon energy $E_\gamma = 100\,\text{MeV}$.

3.4 Pion absorption from the lowest atomic orbital

3.4.1 Pion absorption in ^{2}H

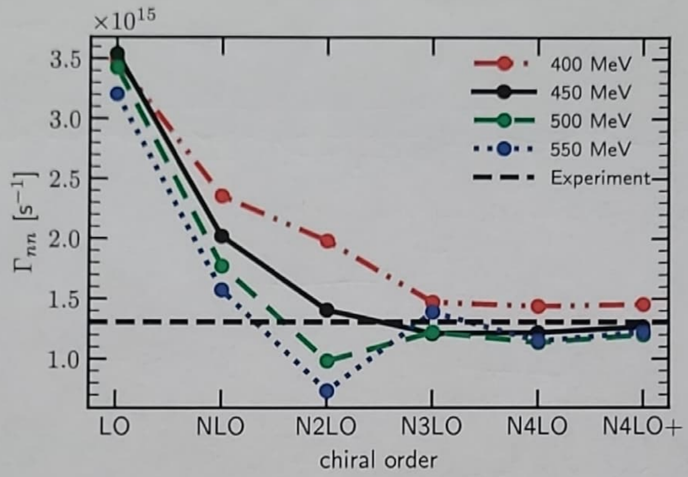

to say that we didn't extract that by ourself.

the

Figure 3.46: Absorption rate for the reaction $\pi^- + {}^2\text{H} \rightarrow n + n$. The rates were calculated using the SMS force with different chiral orders and cutoff values. The results were obtained using the single-nucleon transition operator and including two-nucleon contributions at the leading order. The figure shows the results obtained using plane wave (PW) plus two-neutron rescattering (Full) parts. The experimental value is ~~obtained~~ extracted from the hadronic ground-state broadening in pionic deuterium [?, ?].

and taken from Ref [....]

3.4.2 Pion absorption in ^{3}He

in Fig. 3.47 and 3.48 the pion absorption rates are presented as a function of the chiral order with different values of the cutoff parameter (for $\pi^- +^3\text{He} \rightarrow p+n+n$ and $\pi^- +^3\text{He} \rightarrow n+d$ reactions, respectively). Both figures show that with fixed chiral order the arrangement of values with respect of the cutoff parameter remains the same, namely with increasing Λ, absorption rate decreases. The only exception in both cases appears at N^{3}LO where prediction with $\Lambda = 550\,\text{MeV}$ goes above other predictions. At the next order, N^{4}LO, it corrects to the normal arrangement. This behavior may be connected to the 3NF used for the calculation and in order to check that I show a similar figure for a proton radius r_p in Fig. 3.49 calculated with and without 3NF (left and right panels respectively). Results obtained with 3NF show similar deviation at N^{3}LO while data obtained without 3NF does not have that. Nevertheless, the spread of predictions with respect to the cutoff values is much smaller with 3NF and deviation seems to be not crucial as total difference between predictions in this case is very small.

In Figs. 3.50 and 3.51 I show intensity plots for the double differential absorption rates $d^2\Gamma_{pnn}/dE_1dE_2$ for the $\pi^- +^3\text{He} \rightarrow p+n+n$ process as functions of the nucleons energies (first nucleon is proton) and of *correct naming* Dalitz coordinates(x and y) respectively.

In Fig. 3.51 coordinates x and y are defined as:

3He wave function resulting from the

absorption rates obtained with various values

and for

~~3.3 Pion absorption from the lowest atomic orbital~~

3.3.1 Pion absorption in ^{3}He

In Fig. 3.36 and 3.37 the pion absorption rates are presented as a function of the chiral order ~~with~~ different values of the cutoff parameter (for $\pi^- +^3 He \rightarrow p+n+n$ and $\pi^- +^3 He \rightarrow n+d$ reactions, respectively). Both figures show that with fixed chiral order the arrangement of ~~values with respect~~ of the cutoff parameter remains the same, namely with increasing Λ, absorption rate decreases. The only exception in both cases appears at N^{3}LO where prediction with $\Lambda = 550$ MeV goes above other predictions. At the next order, N^{4}LO, it ~~corrects~~ comes back to the ~~normal~~ usual arrangement. This behavior may be connected to the 3NF used for the calculation ~~and~~ In order to check that I show a ~~similar~~ corresponding figure for a proton radius r_p $\boxed{\text{in Fig. 3.38}}$ calculated with and without 3NF (left and right panels respectively). Results obtained with the 3NF show similar deviation at N^{3}LO while ~~data~~ obtained without the 3NF does not ~~have that~~. Nevertheless, the spread of predictions with respect to the cutoff values is much smaller with 3NF and deviation seems to be not crucial as total ~~difference between~~ predictions in this case is very small.

OK

3He

radius

seen in Fig 3.38

→ use font like in ~~previous~~ Fig for deuteron

Write about size of spread in different orders. Give numbers in % for N2LO, N4LO, N4LO+

is there a difference?

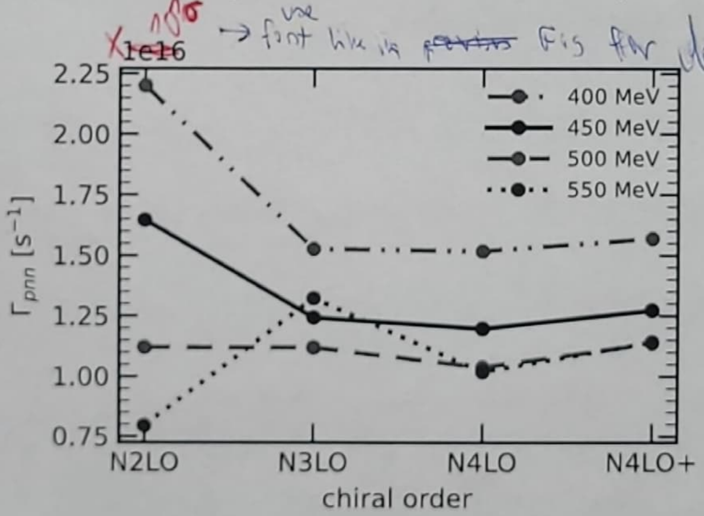

Figure 3.36: Absorption rate for $\pi^- +^3 He \rightarrow p+n+n$ reaction as a function of the chiral order with different values of the cutoff parameter Λ. Predictions were obtained with ~~3NF~~. and the same NN interaction at given order combined with N^{2}LO 3NF.

write

In Figs. 3.39 and 3.40 I show intensity plots for the double differential absorption rates $d^2\Gamma_{pnn}/dE_1dE_2$ for the $\pi^- +^3 He \rightarrow p+n+n$ process as functions of the nucleons energies ~~(first nucleon is proton)~~ and of ~~correct naming~~ Dalitz coordinates (x and y), respectively. ~~In Fig. 3.40~~ The coordinates x and y are defined as:

(assuming nucleon no 1 to be proton)

$$
\begin{aligned}
x &= 3(E_1 + 2E_2 - E)/E, \\
y &= (3E_1 - E)/E,
\end{aligned}
\tag{3.4}
$$

where E is ...

They — taking the region where $r^2 \equiv x^2 + y^2 \leq 1$.

Each of two figures consists of four panels representing predictions obtained with different values of the cutoff parameter Λ. The difference between predictions which can be noticed with the naked eye - is that area of the central region (corresponding to

intermediately

By its nature the total absorption rates cann't deliver details on distribution of ~~various~~ contributions to the absorption process in the phase-space

arising from the various dynamical ingredients

Thus, in following, in Figs. 3.34 – ... I show various intensity plots revealing ~~ranges~~ phase-space regions of special interesting.

Let me remind that in case of absorption rates only two kinematical variables are necessary to define exclusive kinematical configuration. That is, because for that process there is full rotational symmetry, as none of vectors define the z-axis.